Corrosion Science 115 (2017) 93–105

Contents lists available at ScienceDirect

Corrosion Science

journal homepage: www.elsevier.com/locate/corsci

Mechanism of magnetite formation in high temperature naphthenic acid corrosion by crude oil fractions

Peng Jin*, Srdjan Nesic

Institute for Corrosion and Multiphase Technology, Ohio University, 342 West State Street, Athens, OH 45701, USA

ARTICLE INFO

Article history:
Received 23 June 2016
Received in revised form
19 November 2016
Accepted 24 November 2016
Available online 25 November 2016

Keywords:
A. Carbon steel
A. Low alloy steel
B. TEM
C. Acid corrosion
C. High temperature corrosion

ABSTRACT

Naphthenic acids and sulfur compounds present in crude oils may cause corrosion in oil refineries. In some cases, corrosion product scale formed in these oils may provide corrosion protection, but in other cases this may not be true. Current research investigates the nature of protective scales formed on steel corroded by crude oil fractions using microscopic and analytical techniques. This research identifies a thin oxygen-containing layer in-between the steel and a thicker iron sulfide outer layer contributing to the protection against naphthenic acid corrosion. Formation of this oxygen-containing layer is likely due to naphthenic acids in the crude oil.

1. Introduction

Cheaper crude oils – the so called "opportunity crudes", which are characterized by a higher content of corrosive naphthenic acids (NAP) and sulfur compounds, are potentially attractive to refineries. However, their processing may promote refinery corrosion. Therefore, despite their lower cost, processing of opportunity crudes presents potential issues of facility integrity management. Given this background, there is an incentive to investigate and better understand corrosion of steel by NAP and sulfur compounds in order to improve the strategy for corrosion mitigation.

Corrosion by sulfur compounds has been recognized as a problem in the crude oil refining industry for a long time [1]. Among sulfur compounds found in crude oil fractions, mercaptans, sulfides, and disulfides are reactive while thiophenes are relatively stable and are perceived to be noncorrosive. The concentration of NAP in crude oil is commonly denoted by Total Acid Number (**TAN**, the amount of potassium hydroxide (KOH) in mg needed to neutralize acidity in one gram of crude oil). NAP corrosion of steel is not a new phenomenon, either; it has been identified as a challenge for refineries since mid-twentieth century [2]. Therefore, a significant body of research is available in the literature on both types of corrosion and a basic understanding of the process has emerged. The overall corrosion process is often summarized via three reactions, Eqs. (1)–(3) [3]:

$$Fe + 2RCOOH \rightarrow Fe(RCOO)_2 + H_2 \quad (1)$$

$$Fe + H_2S \rightarrow FeS + H_2 \quad (2)$$

$$Fe(RCOO)_2 + H_2S \rightleftarrows FeS\downarrow + 2RCOOH \quad (3)$$

NAP corrosion is generally described by Eq. (1), where R is a generic alkyl group, usually containing at least one saturated ring with five or six members. The corrosion product of NAP corrosion is iron naphthenate ($Fe(RCOO)_2$), which is oil soluble and therefore does not form a surface scale, so it is commonly thought that it does not deter corrosion. Eq. (2) represents corrosion by sulfur compounds, where all the reactive sulfur compounds found in crude oil fractions (mercaptans, sulfides, and disulfides) are represented by H_2S, since these compounds decompose to H_2S at high temperatures. The corrosion product – the solid iron sulfide (FeS), forms a scale on the steel surface (via Eq. (2)) because it is not oil soluble. This scale may provide corrosion protection. However, a clear correlation between the physical and chemical composition of iron sulfide scale and its protective properties has not been found to date. Eq. (3) indicates a possible interaction between the NAP and sulfur species.

Since it is ubiquitous, iron sulfide scale is often attributed to be the main component of corrosion protection. Most of the research efforts in the past focused on the effect of sulfur compounds found in the oil and the conditions which promoted the formation of

* Corresponding author.
E-mail addresses: pj221108@ohio.edu, jinp04@gmail.com (P. Jin).

http://dx.doi.org/10.1016/j.corsci.2016.11.021
0010-938X/

Table 1
Chemical composition of A106 carbon steel (CS) specimen (%wt).

C	Si	Mn	P	S	Cr	Ni	Mo	V	Cu	Fe
0.18	0.41	0.8	0.11	0.06	0.02	0.04	0.02	0.03	0.08	Bal

Table 2
Chemical composition of A182-F5 chromium steel (5Cr) specimen (%wt).

C	Si	Mn	P	S	Cr	Ni	Mo	Cu	Al	Ti	N	Sn	Zr	Fe
0.1	0.24	0.41	0.022	0.005	4.47	0.14	0.5	0.12	0.01	0.006	0.012	0.007	0.002	Bal

protective iron sulfide scales. For instance, Dettman, *et al.*, found that the sulfur compounds in Athabasca bitumen promoted the formation of a protective iron sulfide scale [4]. In other studies, low concentration of H_2S in the gas phase (0.2 psia) was found to lead to the formation of a protective FeS scale, while the corrosion was accelerated by higher concentration of hydrogen sulfide (0.45 psia) [5–7]. In general, reactive sulfur compounds lead to a more complicated behavior than the one described here [7]. Others have postulated that the varied molecular structure and the interference by NAP affect the corrosive or protective nature of the iron sulfide scale [4,8–13].

In our prior publications, an oxygen-containing scale composed of magnetite (Fe_3O_4) adjacent to the steel surface was formed during the corrosion by model NAP [14–20]. The oxygen-containing scale, rather than the iron sulfide scale, was found to be protective against NAP corrosion. It was evidenced that the formation of oxygen-containing scale was dependent on the NAP structure due to the thermal decomposition of iron naphthenate above 250 °C via Eqs. (4) and (5) [21–28]. Thermal decomposition of iron carboxylates at high temperature has been widely applied to prepare nano particles of iron oxides [29–32]. As the initial product, wüstite (FeO) is not stable; it further transfers to other stable forms of iron oxides. Under reducing conditions, magnetite is the final product as shown in Eq. (5). We have found that a continuous magnetite layer with thickness of nanometers was formed during the corrosion by model NAP (simple and pure carboxylic acid).

$$Fe(RCOO)_2 \rightarrow FeO + CO_2 + RCOR \quad (4)$$

$$4FeO \rightarrow Fe_3O_4 + \alpha\text{-}Fe \quad (5)$$

However, structures of indigenous NAP in the crude oil are quite complex [33,34]. Findings for a simple carboxylic acid may not be directly applied to the real crude oil. Moreover, other corrosive component in the crude oil (sulfur compounds, for example) also affected the formation of corrosion product scales. Therefore, it was not clear whether the finding of magnetite formed in a single carboxylic acid can be extended to the real crude oil with complex components.

In the present study, three representative crude fractions were employed to corrode carbon steel and low-chromium steel specimens at high temperatures. The protectiveness of corrosion product scale against NAP corrosion was evaluated. The scale morphology was investigated by Transmission Electron Microscopy (TEM). The chemical composition was determined via Energy Dispersive Spectroscopy (EDS) which was combined with TEM analyses. Convergent Beam Electron Diffraction (CBED) and Selected Area Diffraction (SAD) combined with TEM provided useful information on the crystal structure.

2. Experimental

2.1. Experimental materials

Ring specimens made from A106 carbon steel (CS, the most encountered type of steel in crude oil refineries) and A182-F5 chromium steel (5Cr, still found in some refineries) were utilized in the experiments and their chemical compositions are listed in Tables 1 and 2, respectively. For each ring specimen, the outer diameter was 81.76 mm; inner diameter 70.43 mm; and height 5.00 mm. For repeatability, each steel specimen is abraded by 400 and 600 grit silicon carbide (SiC) paper in succession under the flow of isopropanol to minimize oxidation in air immediately prior to each experiment. These specimens are then rinsed with toluene and acetone, dried under N_2 flow, and weighed on a scale with the accuracy of 0.1 mg.

2.2. Experimental fluids

As shown in Table 3, three conventional crude oil fractions were used to corrode steel specimens and generate corrosion product scales. Fraction 1 is a vacuum gas oil (VGO) slate of a heavy crude oil sampled from a refinery, having a high TAN/lower sulfur content. Fraction 2 is a VGO blend extracted from a refinery. Fraction 3 is representative of a heavy crude oil fraction, being a residue from the atmospheric distillation, collected at 343 °C in a refinery. In addition to TAN and sulfur content, Table 3 shows the content of asphaltenes in these crude oil fractions. Asphaltenes refer to large-molecule hydrocarbon compounds in the crude oil that are not soluble in heptane but can dissolve in toluene [35]. It is known that asphaltenes can affect corrosion of steel in the presence of liquid water in the transfer pipelines of crude oil at room temperature [36]. In our prior research, it was evidenced that asphaltenes did not affect the high-temperature corrosion by crude oil fractions [16]. The content of water and chloride which affect the room-temperature corrosion is unknown but expected to be negligible, given that these crude oil fractions were extracted from high-temperature distillation well above the boiling point of water. In our prior research, water was intentionally added into the fluid, but no corrosive effect was found under similar conditions as the current study [16]. Therefore, the current study focused on NAP (characterized by TAN) and sulfur compounds (characterized

Table 3
Composition and properties of real crude fractions.

Parameter	Fraction 1	Fraction 2	Fraction 3
TAN (mg KOH/g oil)	4.9	1.75	1.06
Sulfur content (%wt)	0.11	0.53	4.29
Asphaltenes content (%wt)	0.05	0	14.9
Aromatics content (%wt)	58	64	54.4
Naphthenes content (%wt)	35	17	7.6
Paraffins content (%wt)	6	18	23
Density at 15° C (g/cm^3)	0.819	0.795	0.822
Appearance	Black	Green	Black

by sulfur content) which were widely investigated regarding their high-temperature corrosive effects [2–8].

In order to assess the protectiveness, scales formed in real crude fractions were attacked by a corrosive solution prepared by dissolving a mixture of NAP available from TCI Americas (TCI) in a high boiling white mineral oil (TAN 3.5) [14].

2.3. Experimental equipment

Two types of equipment were used in the experiment – the closed stirred autoclave and the High Velocity Rig (HVR). The autoclave was filled with a crude oil fraction to corrode steel specimens. During the experiment, the crude oil fraction was stirred to enhance heat transfer while specimens were stagnant. HVR was a flow-through system with specimens mounted in the HVR reactor. During the experiment, specimens were rotated at 2000 rpm with the corrosive TAN 3.5 solution flowing over them. Schemes of autoclave and HVR can be found in our prior publications [14–19].

2.4. Experimental procedures

There were two steps in experimental procedures – the **pretreatment** and the **challenge**.

2.4.1. Pretreatment

In order to vary the protective properties of the surface scales, specimens are first exposed to a given crude oil fraction in the stirred autoclave experiment. Specimens were immersed in the crude oil fraction, the stirred autoclave was closed and the crude oil fraction was purged by nitrogen to remove oxygen. Then, the autoclave was heated and kept at a designated temperature, usually at 316 °C or 343 °C according to the processing temperature to obtain the corresponding crude oil fraction. This part of the experimental procedure was named "pretreatment" and lasted for 24 h. This time duration was determined experimentally to be long enough for the corrosion product scale to form on the specimen surface and for the corrosion rate to stabilize.

Following each pretreatment experiment, the corrosion rate was determined by weight loss. To this end, the scale formed on the steel surface was removed by immersing the specimens for 20 s in the "Clarke" solution, made according to the ASTM G 1–03 and reweighed. This scale removal step was repeated multiple times until the difference of successive weights was less than 5 mg. The final weight of specimens was used to calculate the weight loss due to corrosion in the pretreatment step of the experiment. The 5 mg error in weighing was deemed acceptable as it amounted to an error in corrosion rate calculation <0.02 mm/y.

To assess the true protectiveness and tenacity of scale formed in the pretreatment step, another parallel pretreatment was ran and the specimens with their intact scales were subsequently transferred to HVR. The corrosive TAN 3.5 solution was fed into the HVR and the temperature was kept at 343 °C, resulting in a harsh environment in which the protectiveness of scale was "challenged". This step was called "challenge" as described below. The "challenge" step was also described and implemented in our prior publications [14–20].

2.4.2. Challenge

As soon as the pretreated specimens were extracted from the stirred autoclave, they (with their scale in-place) were transferred to the HVR. The HVR was continuously refreshed with the corrosive TAN 3.5 solution at a flow rate of 7.5 cm^3/min. The temperature in the HVR reactor was kept at 343 °C and specimens were rotated at 2000 rpm which corresponded to a peripheral velocity of 8.5 m/s and a shear stress of 74 Pa. It was considered that in such an aggressive environment, the scale formed on specimens in the pretreatment step was "challenged" for 24 h in order to examine its protectiveness against NAP attack. Following each pretreatment/challenge experiment, the corrosion rate was determined by weight loss.

As a control experiment, fresh steel specimens (without any pretreatment) were corroded in the HVR under the same condition as listed above. The bare surface corrosion rate is measured and referred to as "bare steel TAN 3.5 corrosion rate". It was expected that if the scale formed in the pretreatment step was protective, the challenge corrosion rate would be lower than the bare steel TAN 3.5 corrosion rate.

High-resolution TEM was utilized to analyze the specimens at a high magnification. The TEM analysis was conducted on a FEI Tecnai F20XT operating in the Scanning Transmission Electron Microscopy (STEM) mode and a Phillips CM200 TEM with a double tilt holder. The achievable resolution is as high as 0.18 nm, which is sufficient to reveal the structure of very thin scales. The EDS detector equipped with TEM was used to indicate the elemental distribution within the scale. Additionally, CBED and SAD combined with TEM helped reveal the crystalline structure of compounds found in the scale. X-Ray Diffraction (XRD) analysis was performed on Rigaku Miniflex II XRD using Cu Kα radiation.

2.5. Evaluation of corrosion rates

Corrosion rate of steel specimens was calculated for the two different steps of the experiment based on the corresponding weight loss. Eq. (6) was applied to calculate the corrosion rate in the pretreatment step. The pretreatment step was executed twice: once to make a measure of the weight loss without preserving the scale and a second time without weight loss measurement but the scale was preserved. The pretreated specimens (with their scale in-place) were extracted from the stirred autoclave, transferred to the HVR which was refreshed with the corrosive TAN 3.5 solution. It was the challenge step. The challenge corrosion rate was calculated by subtracting the weight loss found in the pretreatment step from the overall weight loss in the challenge step (Eq. (7)).

$$V_1 = \frac{87600\Delta W_1}{\rho A_1 t} \tag{6}$$

$$V_2 = \frac{87600(\Delta W_2 - \Delta W_1)}{\rho A_2 t} \tag{7}$$

In Eqs. (6) and (7), V_1 is the pretreatment corrosion rate, mm/y; V_2 is the challenge corrosion rate, mm/y; 87600 is the unit conversion constant; ΔW_1 is the weight loss in the pretreatment step, g; ΔW_2 is the weight loss in the challenge step, g; ρ is the density of ring specimen, g/cm^3; A_1 is the area of ring specimen exposed to pretreatment solution during the pretreatment, cm^2; A_2 is the area of ring specimen exposed to corrosive TAN 3.5 solution during challenge, cm^2; t is the corrosion time, h.

3. Results

3.1. Crude oil fraction 1

Corrosion rates of CS and 5Cr specimens, pretreated with Fraction 1 at 316 °C, are shown in Table 4. Recall, that Fraction 1 is a high-TAN/low-sulfur crude oil fraction, and that low corrosion rates in the pretreatment step are seen for both metallurgies. This is counter to the conventional understanding where the high TAN indicated a high NAP concentration leading to high corrosion rates in the pretreatment step and any retardation by a sulfide scale was not expected due to the low sulfur content [2].

Challenge corrosion rates of both steels, shown in Table 4, are low, especially for the 5Cr steel. Furthermore, for both steels the

Table 4
Summary of pretreatment and challenge corrosion rates for CS and 5Cr steel specimens pretreated in Fraction 1. In each experiment, three specimens of each metallurgy were used for weight loss analysis to measure corrosion rates. Corrosion rates are presented in the following format: average corrosion rate (maximum corrosion rate, minimum corrosion rate).

Metallurgy	Pretreatment Corrosion Rate (mm/y)	Challenge Corrosion Rate (mm/y)	Bare Steel TAN 3.5 Corrosion Rate (mm/y)
CS	0.1 (0.1, 0.1)	3.1 (4.5, 1.6)	7.8 (8.1, 7.6)
5Cr	0.1 (0.1, 0.1)	0.1 (0.1, 0.1)	1.8 (2.0, 1.6)

challenge corrosion rate is much lower than the corresponding bare steel TAN 3.5 corrosion rates, suggesting that protective scales were formed during the pretreatment with Fraction 1. This result is counter to the common wisdom – that a high-TAN/low-sulfur crude oil fraction would not form a scale on the metal surface, let alone a protective one. To find the cause of this unexpected behaviour, the scales formed on the steel specimens pretreated with Fraction 1 were investigated by TEM.

The TEM image of the thin scale formed on CS specimen during the pretreatment in Fraction 1 is shown in Fig. 1. A scale, 0.35 μm in thickness, is clearly visible, having a coarser structure adjacent to the steel surface ("inner" layer). The EDS analysis of this scale is shown in Fig. 2, and clearly suggests that there are two layers of the scale with different chemical composition. The EDS scan was performed on consecutive points along the white line (from the bottom to the top) in Fig. 1 and the first point was located in the steel matrix. Given that the EDS analysis on light atoms such as oxygen is not as accurate as that for heavy atoms such as iron, the change of oxygen content in different points is more meaningful that the absolute content given by the EDS detector. As shown in Fig. 2, the detected oxygen content in the outer layer is close to that in the steel matrix and sulfur content increases to become nearly equimolar with that of iron. In the CBED patterns (Fig. 5), only the diffraction pattern of triolite (not the iron oxide) is found in the outer layer. Thus, it was concluded that the "detection" of oxygen in the outer layer was an artifact. Therefore, the TEM analysis indicates that there is a thin oxygen-containing layer adjacent to the steel surface covered by an iron sulfide layer.

The scale formed under the same conditions on 5Cr steel, which was more protective against NAP corrosion, looks somewhat different, as revealed in the TEM image shown in Fig. 3. Two distinct layers in the scale are visible with a sharp boundary between them.

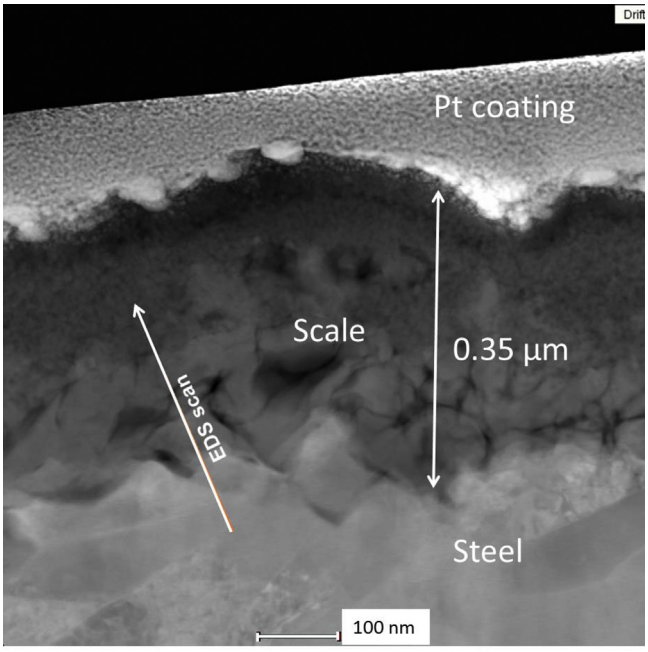

Fig. 1. Transmission Electron Microscopy (TEM) image – cross-section of CS specimen pretreated in Fraction 1. The white line indicates the location of the Energy Dispersive Spectroscopy (EDS) scan shown in Fig. 2 below.

The thickness of the inner layer is around 0.25 μm. When the position of the original steel surface is reconstructed from weight loss measurements it appears to be also about 0.25 μm from the steel surface, as shown in Fig. 3, placing it very close to the boundary between the two layers of the scale. Results of EDS analysis of the same scale, shown in Fig. 4, indicate that the outer layer of the scale is most likely iron sulfide while the inner layer is an iron oxide scale since it contains no sulfur. The chemical composition of the inner layer for 5Cr steel is similar to that seen on CS, and the only major difference is in the elevated chromium content. It is hypothesized that the presence of chromium in the scale is significant to enhance the scale protectiveness.

The CBED patterns generated for CS and 5Cr specimens (shown in Figs. 5 and 6 respectively) clearly demonstrate the crystalline structures of the components of the inner and outer layers of the scales. The bright field TEM images in Figs. 5 and 6 show the location

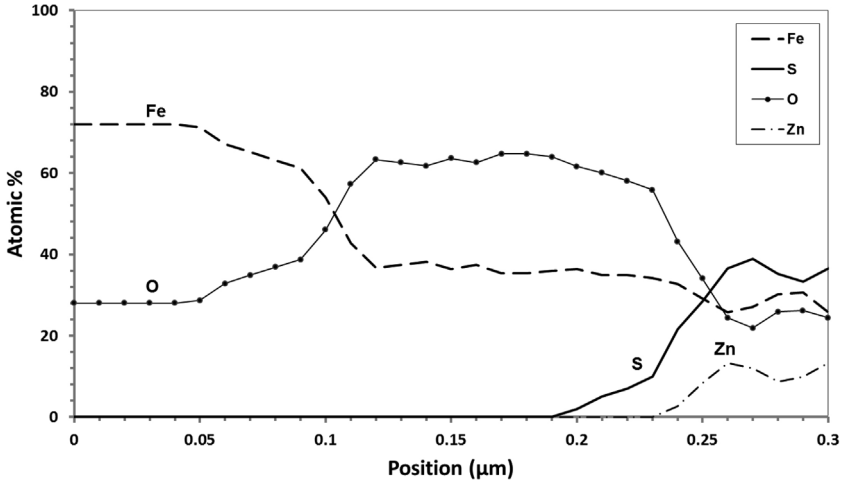

Fig. 2. Elemental profile of the cross-section CS specimen pretreated in Fraction 1 (Transmission Electron Microscopy (TEM) image presented in Fig. 1). The Energy Dispersive Spectroscopy (EDS) analysis was performed along the white line in Fig. 1 from the bottom to the top and contains all detected elements. All other elements are of negligible concentration.

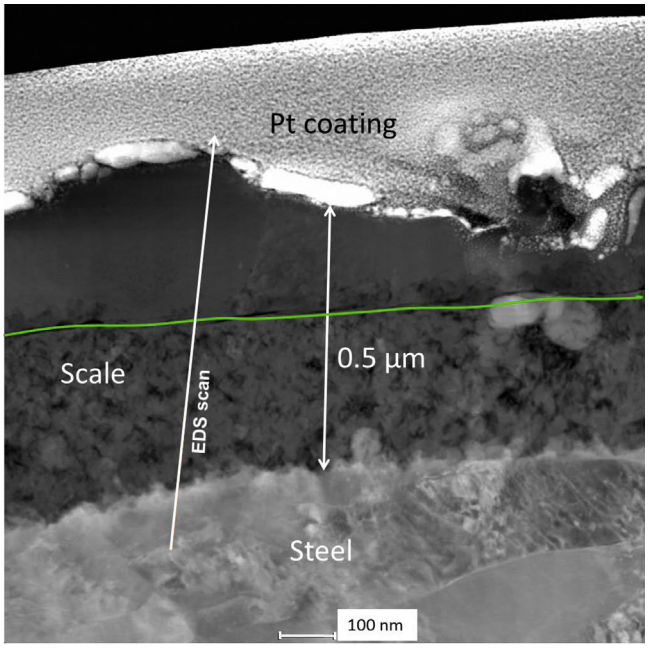

Fig. 3. Transmission Electron Microscopy (TEM) image – cross-section of 5Cr specimen pretreated in Fraction 1. The white line indicates the location of the Energy Dispersive Spectroscopy (EDS) scan shown in Fig. 4 below. The thick green line shows the original steel surface reconstructed from weight loss measurements. (For interpretation of the references to colour in this figure legend, the reader is referred to the web version of this article.)

for the CBED analysis and indicate that both layers are dense. Given the elemental profile shown in Figs. 2 and 4, it is determined that the outer layer is composed of troilite (FeS) while magnetite (Fe_3O_4) is the major component of the inner layer for both CS and 5Cr steel.

3.2. Crude oil fraction 2

Fraction 2 is a crude oil fraction with medium content of both NAP and sulfur compounds (TAN 1.75, sulfur content 0.53%wt). It forms a protective scale on the surface of CS specimens during the pretreatment (343 °C) step that resisted the TAN 3.5 challenge, as evidenced by the challenge corrosion rate shown in Table 5. Additionally, the challenge corrosion rate for 5Cr was close to zero, suggesting that the scale was very protective.

Table 5
Summary of pretreatment and challenge corrosion rates for CS and 5Cr steel specimens pretreated in Fraction 2. In each experiment, three specimens of each metallurgy were used for weight loss analysis to measure corrosion rates. Corrosion rates are presented in the following format: average corrosion rate (maximum corrosion rate, minimum corrosion rate).

Metallurgy	Pretreatment Corrosion Rate (mm/y)	Challenge Corrosion Rate (mm/y)	Bare Steel TAN 3.5 Corrosion Rate (mm/y)
CS	0.3 (0.3, 0.3)	0.7 (0.8, 0.5)	7.8 (8.1, 7.6)
5Cr	0.2 (0.2, 0.2)	0.1 (0.1, 0.1)	1.8 (2.0, 1.6)

The TEM analysis of scale formed on the CS specimen provides detailed information on its morphology (Fig. 7). The TEM image shows three distinct layers formed on the metal surface with a total thickness around 1.7 µm. The EDS analysis of scale formed in Fraction 2 suggests that the outer layer is composed of iron sulfide while the iron oxide is the major component in the inner layers (Fig. 8), similar to what was seen with Fraction 1. The analysis also indicates that oxygen is most abundant in the scale layer adjacent to the steel.

The scale morphology for the 5Cr specimen obtained via a TEM analysis is shown in Fig. 9. The inner and outer layers are stacked compactly, without any gaps or cracks. Compared with the scale seen on the CS specimen shown in Fig. 7, the 5Cr steel specimen has a thicker inner layer. The EDS analysis (Fig. 10) reveals similar findings to those seen for the CS specimens – an oxygen-containing layer firmly attached to the steel surface covered with a thinner iron sulfide layer. Moreover, it seems the inner layer is composed of two sublayers – one rich in iron oxide and one with a mixed iron oxide/iron sulfide composition.

After the challenge, the overall integrity of the scale formed on the 5Cr steel specimens are preserved (Fig. 11), even if the outer iron sulfide layer is barely visible and is removed probably due to the combined effect of corrosive NAP and high velocity. However, the oxygen-containing layer survives and presumably protects the steel. In Figs. 10 and 11, the "detected" oxygen content in initial point of EDS scan located in the steel matrix is about 6% and 43%, respectively. As explained above, the EDS analysis on oxygen is not quite accurate and the change of oxygen content in different points is more meaningful. The absolute oxygen content measured by the EDS detector may be determined by the calibration of instrument, the thickness of TEM sample, and the sample storage time. The oxygen content "detected" in the steel matrix can serve as the

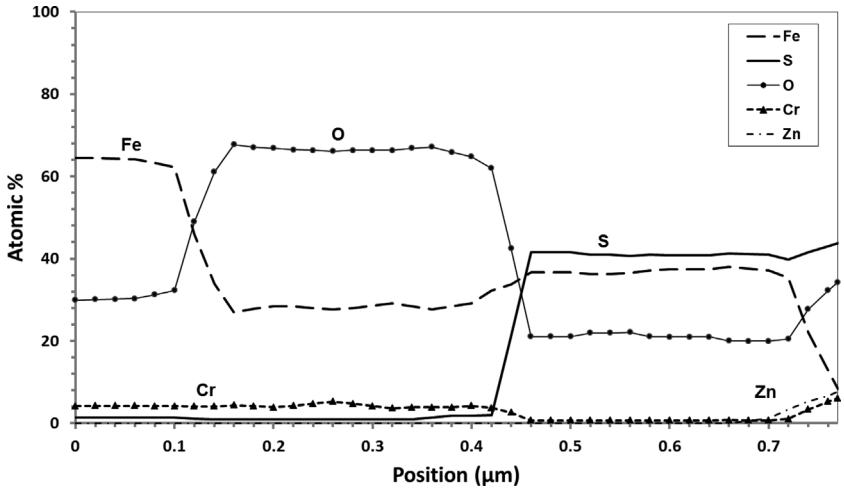

Fig. 4. Elemental profile of the cross-section 5Cr specimen pretreated in Fraction 1 (Transmission Electron Microscopy (TEM) image presented in Fig. 3). The Energy Dispersive Spectroscopy (EDS) analysis was performed along the white line in Fig. 3 from the bottom to the top and contains all detected elements. All other elements are of negligible concentration.

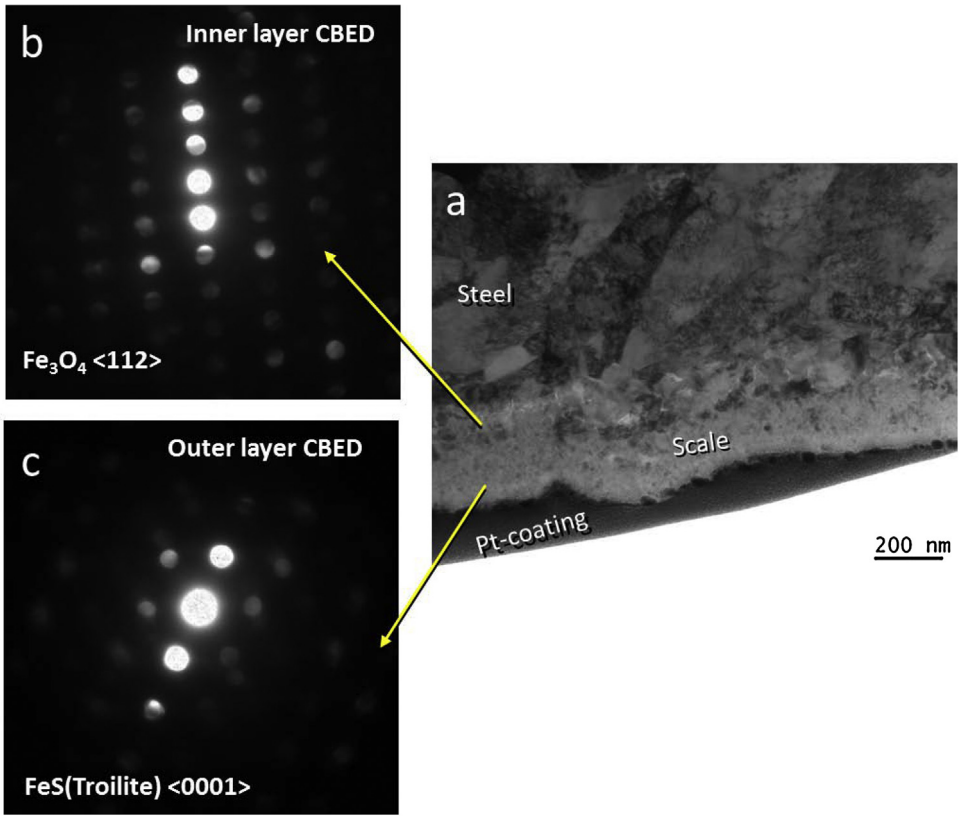

Fig. 5. Transmission Electron Microscopy (TEM) image (a) and Convergent Beam Electron Diffraction (CBED) patterns (b and c) of scales formed on CS specimen after pretreatment in Fraction 1.

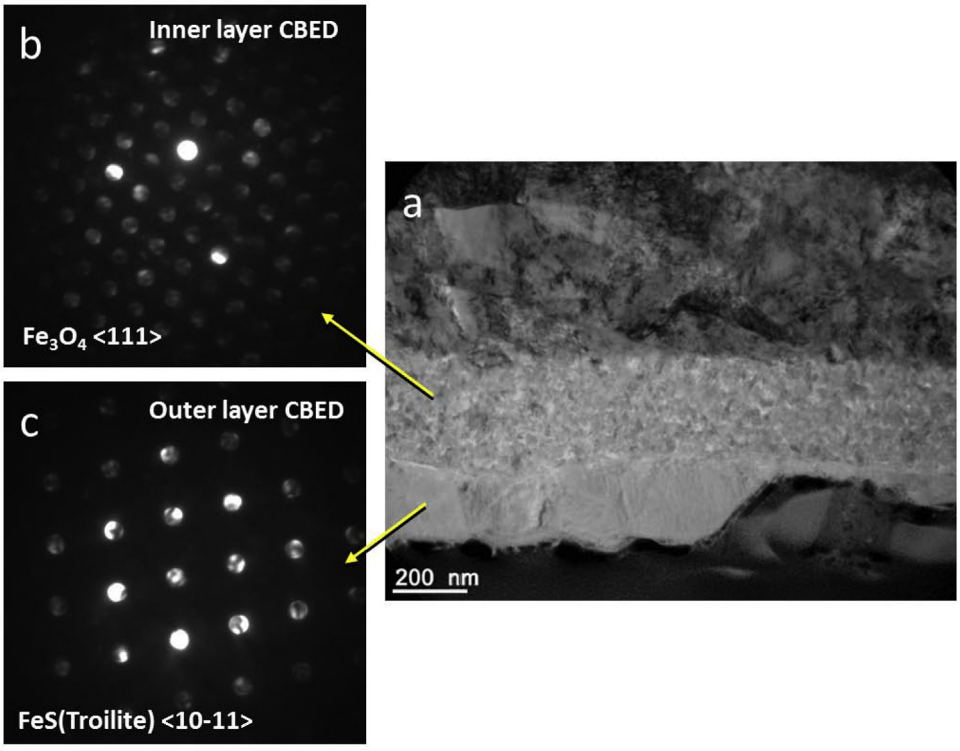

Fig. 6. Transmission Electron Microscopy (TEM) image (a) and Convergent Beam Electron Diffraction (CBED) patterns (b and c) of scales formed on 5Cr specimen after pretreatment in Fraction 1.

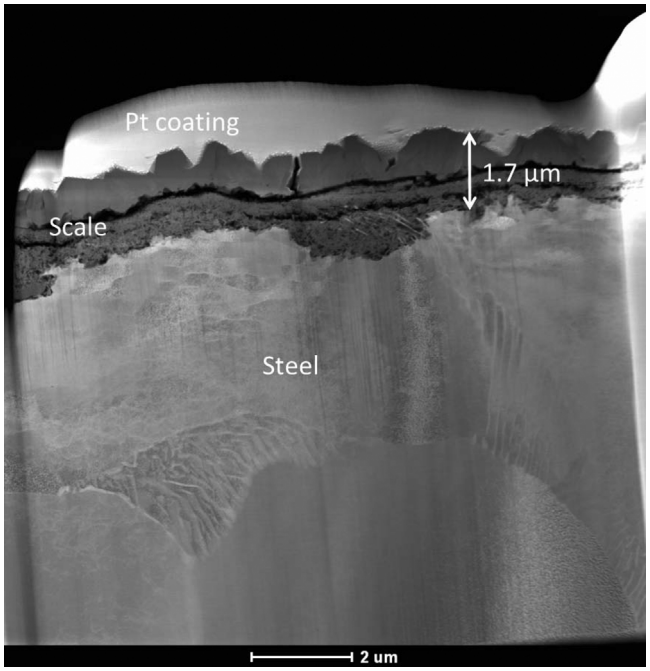

Fig. 7. Transmission Electron Microscopy (TEM) image – cross section of CS specimen pretreated in Fraction 2.

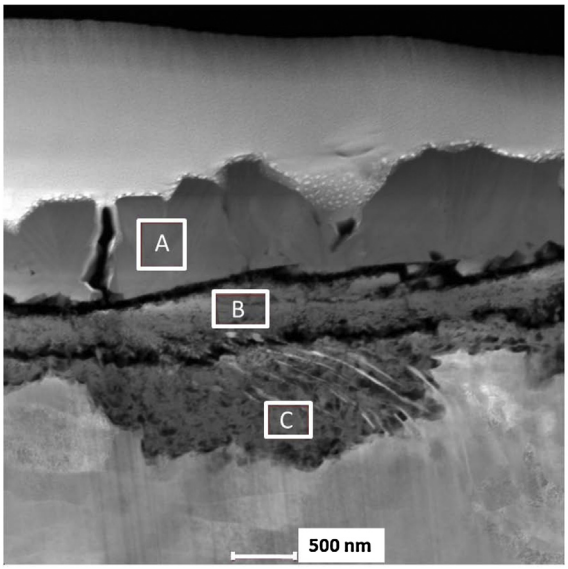

A

Element	Atomic%
S	48.11
Fe	51.88

B

Element	Atomic%
O	21.34
S	23.56
Fe	39.70

C

Element	Atomic%
O	43.54
S	8.39
Fe	41.45

Fig. 8. Energy Dispersive Spectroscopy (EDS) analysis on selected area of the scale formed on CS specimen after pretreatment in Fraction 2 (Transmission Electron Microscopy (TEM) image presented in Fig. 7).The Energy Dispersive Spectroscopy (EDS) analysis was performed in the white area shown in the Transmission Electron Microscopy (TEM) image and contains all detected elements. All other elements are of negligible concentration.

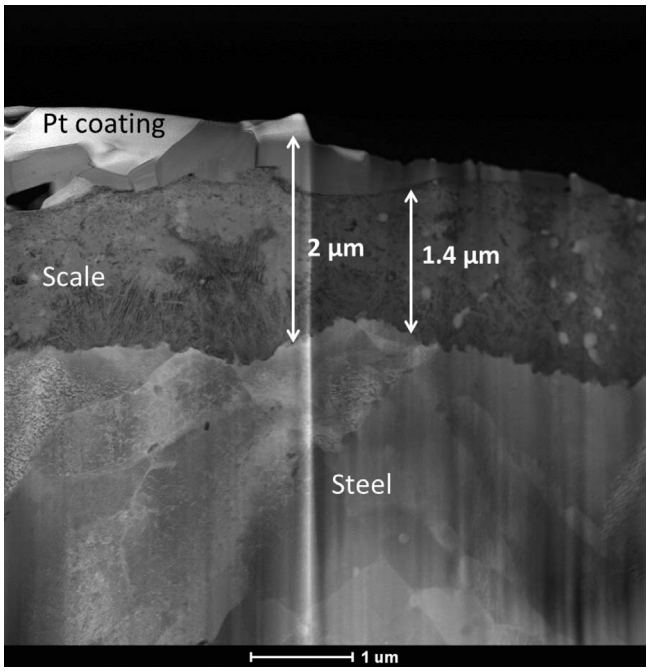

Fig. 9. Transmission Electron Microscopy (TEM) image – cross section of 5Cr steel specimen pretreated in Fraction 2.

Table 6
Summary of pretreatment and challenge corrosion rates for CS and 5Cr steel specimens pretreated in Fraction 3. In each experiment, three specimens of each metallurgy were used for weight loss analysis to measure corrosion rates. Corrosion rates are presented in the following format: average corrosion rate (maximum corrosion rate, minimum corrosion rate).

Metallurgy	Pretreatment Corrosion Rate (mm/y)	Challenge Corrosion Rate (mm/y)	Bare Steel TAN 3.5 Corrosion Rate (mm/y)
CS	0.9 (1.1, 0.8)	1.3 (2.3, 0.7)	7.8 (8.1, 7.6)
5Cr	0.9 (1.1, 0.8)	0.8 (1.7, 0.3)	1.8 (2.0, 1.6)

"background" level of oxygen. In both Figs. 10 and 11, the oxygen content in the inner layer is significantly higher than that in the steel matrix, clearly indicating the presence of oxide.

Results of electron diffraction analysis (Figs. 12 and 13) reveal the presence of magnetite on 5Cr steel after the pretreatment as well as after the challenge. All this strengthens the hypothesis that the protective effect of the scale is primarily related to the well attached inner oxygen-containing layer rather than the outer iron sulfide layer. In the inner layer formed during the pretreatment, sulfur was enriched in the area adjacent to the steel surface as shown in Fig. 10. After the challenge, sulfur was found in the interface between the inner layer and the fluid (Fig. 11). This may be due to the solid state diffusion of sulfur atoms through the inner layer. The solid state diffusion of atoms in the corrosion product layer during the high-temperature corrosion is being studied in on-going research of our group.

3.3. Crude oil fraction 3

Fraction 3 (TAN 1.06, sulfur content 4.29 wt%) is a medium TAN/high sulfur oil. As shown in Table 6, the corrosion rates during the challenge for both CS and 5Cr steel specimens pretreated in Fraction 3 at 316 °C are reduced significantly compared with corresponding bare steel TAN 3.5 corrosion rates, suggesting that this crude oil fraction also promoted the formation of a protective scale. The protective effect of the scale is more pronounced

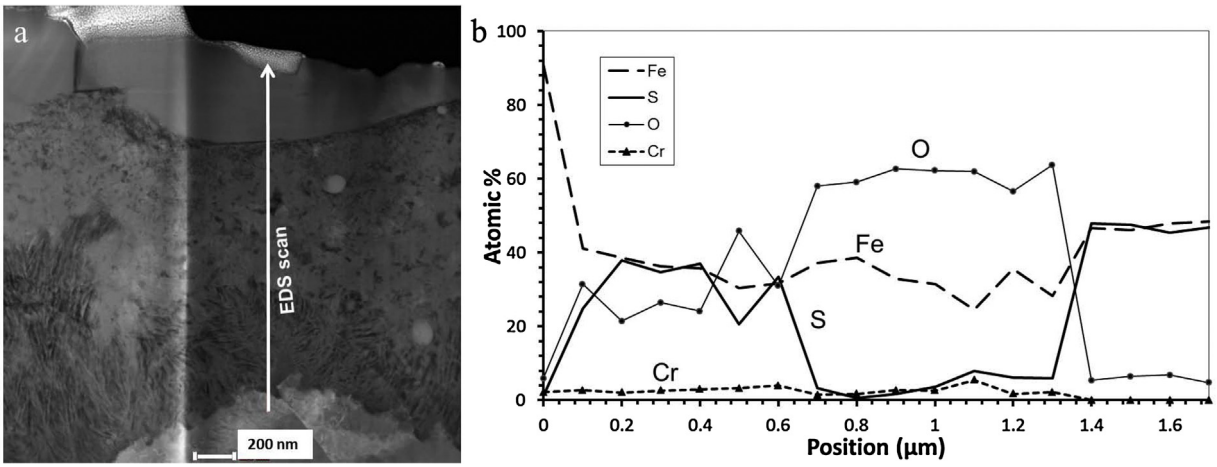

Fig. 10. Elemental profile of the cross-section 5Cr specimen pretreated in Fraction 2 (Transmission Electron Microscopy (TEM) image presented in Fig. 9). (a) Image of scale with the Energy Dispersive Spectroscopy (EDS) scanning line; (b) Results of EDS analysis containing all detected elements. All other elements are of negligible concentration.

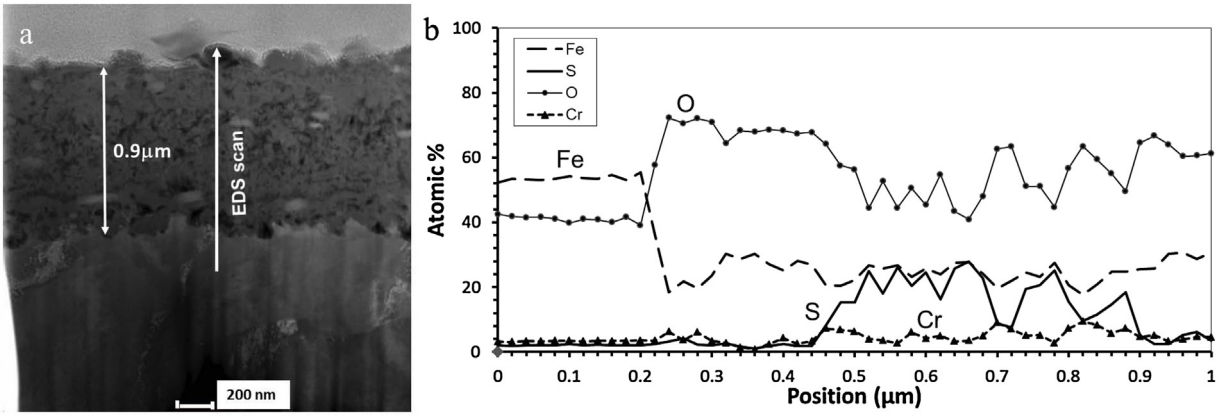

Fig. 11. Transmission Electron Microscopy (TEM)/Energy Dispersive Spectroscopy (EDS) analysis of cross-section 5Cr specimen pretreated in Fraction 2 and challenged with the corrosive TAN 3.5 solution. (a) TEM image of scale with the EDS scanning line from the bottom to the top; (b) Results of EDS analysis containing all detected elements. All other elements are of negligible concentration.

for CS specimens where the challenge corrosion rate was only one sixth of the bare steel TAN 3.5 corrosion rate. Therefore, the following microscopic analysis focuses on the scale formed only on CS specimens.

The TEM image (Fig. 14) shows that the outer layer is truly delaminated. The TEM/EDS analysis suggests that only iron sulfide is present in the outer layer (Fig. 15). There seems to be no distinct boundary between the thin inner layer and the substrate steel. The EDS scan analysis (Fig. 16) indicates that both sulfur and oxygen content increase from 0 to 20% in the inner scale. It should be noted that content of oxygen increases gradually way from the steel while the sulfur seems to be present in bands.

The electron diffraction analysis on the inner layer was not possible due the thickness of the TEM sample. Alternatively, XRD analysis was conducted on the scale formed on this CS specimen and peaks corresponding to troilite (FeS) and magnetite (Fe_3O_4) are detected (Fig. 17). Consistent with previous observations it is assumed that magnetite resides mostly in the inner layer of the scale which is deemed to be a key to the protectiveness against NAP corrosion.

4. Discussion

The presence of an oxygen-containing layer has been reported previously when analyzing the corrosion products on steel specimens corroded under refinery conditions. For instance, iron oxide has been observed by XRD and X-ray Photoelectron Spectroscopy (XPS) analysis of steel surfaces corroded in a crude oil fraction [37]. In a different study, a high-TAN crude oil fraction left a scale of magnetite, which was revealed by XRD analysis [38]. Magnetite was also found on steel surface of samples exposed to white oil containing model sulfur compounds and NAP [12]. In all these cases, the formation of magnetite was deemed to be a laboratory artefact, and it was assumed to be the result of accidental contamination of steel samples, or oxidation in air, or due to unknown components in the crude oil [38]. Even in our previous research from 2006, when magnetite was observed on steel samples it was considered to be an artefact and no significance was assigned to its presence. At that time, the source of this oxygen "contamination" was investigated by intentionally introducing air and/or water into the experiments, but the results were not conclusive and corrosion rates did not respond; therefore this line of investigation was abandoned.

The current results clearly show that that a very thin oxygen-containing layer systematically forms in the three crude oil fractions originating from very different sources, with different TAN, and on both steel types. In all cases where corrosion protection occurs, a thin oxygen-containing layer is found firmly attached to the steel surface, most often covered by an iron sulfide layer. After the challenge with a solution of NAP, the outer iron sulfide layer is removed while the inner oxygen-containing layer is still intact. Therefore, it is postulated that the thin oxygen-containing layer

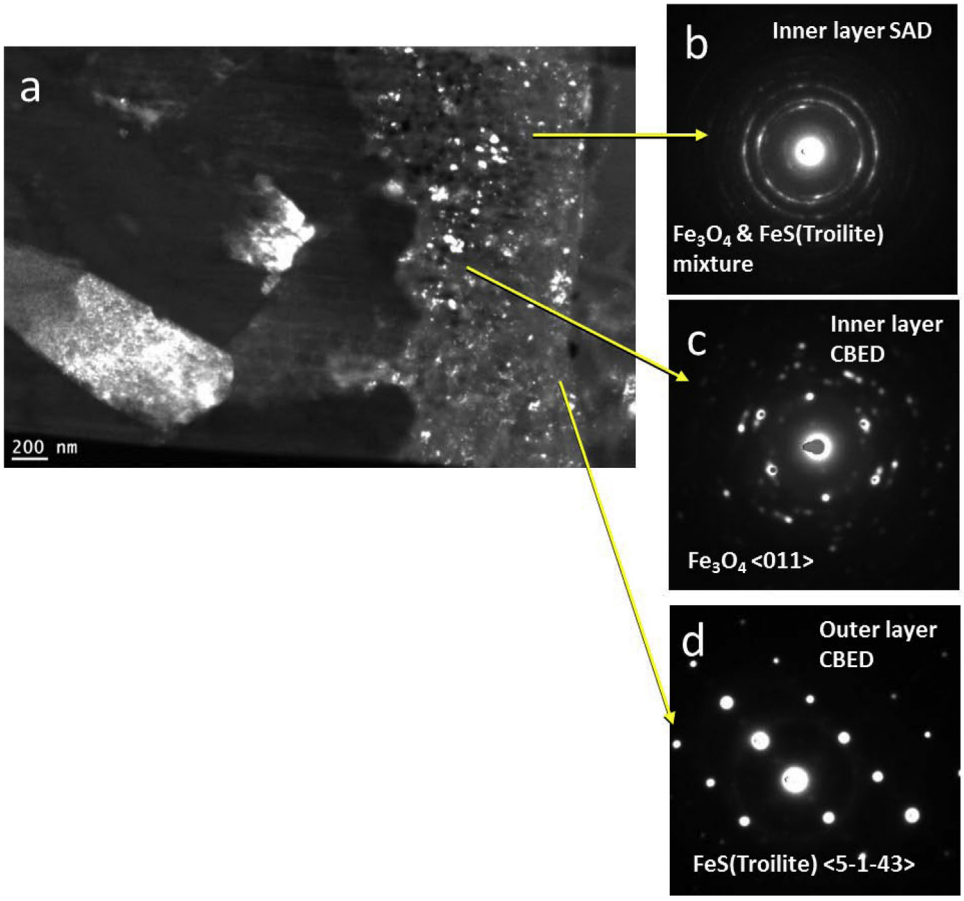

Fig. 12. Transmission Electron Microscopy (TEM) image (a), Selected Area Diffraction (SAD) pattern (b), and Convergent Beam Electron Diffraction (CBED) pattern (c and d) of scale formed on 5Cr specimen pretreated in Fraction 2.

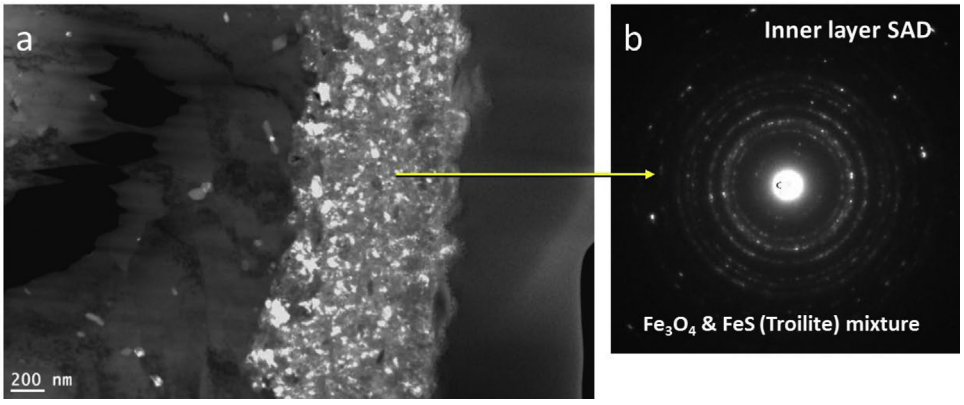

Fig. 13. Transmission Electron Microscopy (TEM) image (a) and Selected Area Diffraction (SAD) pattern (b) of the inner layer formed on 5Cr specimen pretreated in Fraction 2 and challenged with the corrosive TAN 3.5 solution.

contributes to the protection and that formation of magnetite is related to the NAP found in these crude oil fractions.

In order to further verify the mechanism for the formation of oxygen-containing layer during the corrosion by crude oil fractions, steel specimens were pretreated with a solution which was composed of model compounds and had the same TAN and content of corrosive sulfur compounds as Fraction 2. The solution was prepared by dissolving TCI and n-dodecyl sulfide (DDS) in the mineral oil and named as TCI + DDS. After the pretreatment at 343 °C, the scale formed by model compounds was also challenged by the corrosive TAN 3.5 solution to examine its protectiveness.

Comparing with Fraction 2, TCI + DDS did not promote the formation of protective scale for CS specimens (Table 7). However, the scale formed on 5Cr specimens was protective and TEM/EDS analysis suggested that it composed an outer layer of iron sulfide and an inner layer containing oxygen, which was consistent with the composition and morphology of the scale formed in Fraction 2 (Fig. 10 vs. Fig. 18). After the challenge with corrosive TAN 3.5 solution, the protective oxygen-containing layer on 5Cr specimens was preserved (Fig. 19).

Comparing with the magnetite layer formed in the corrosion by a pure carboxylic acid (model NAP) as reported in our prior pub-

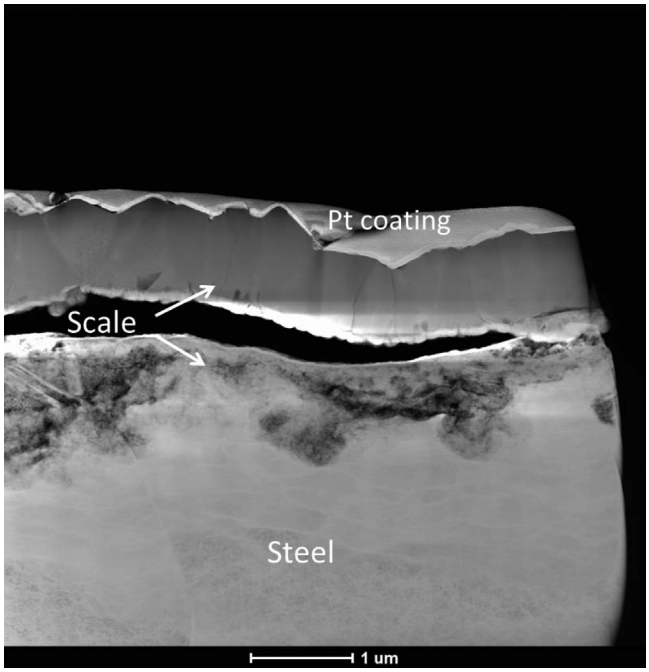

Fig. 14. Transmission Electron Microscopy (TEM) image – cross section of CS specimen pretreated in Fraction 3.

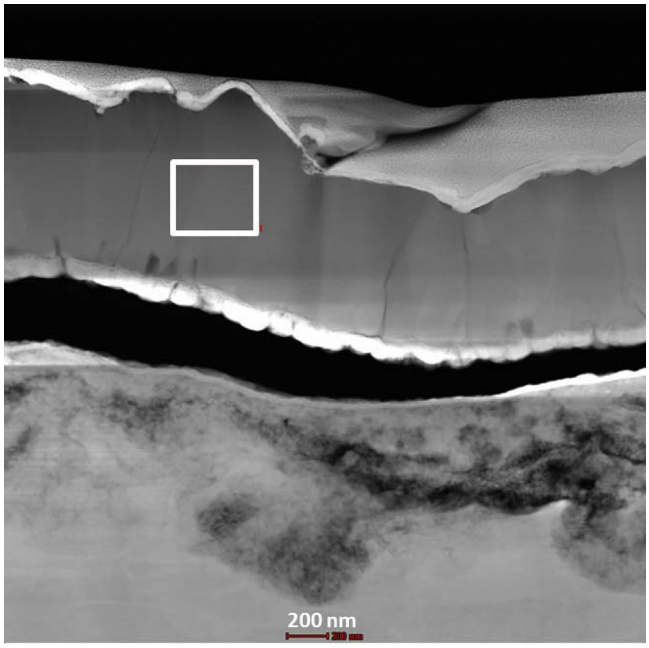

Element	Atomic%
S	23.83
Fe	58.18
C	17.99

Fig. 15. Transmission Electron Microscopy (TEM)/Energy Dispersive Spectroscopy (EDS) analysis of the outer scale formed on CS specimen pretreated in Fraction 3. EDS analysis was performed in the white area shown in the TEM image and contains all detected elements. All other elements are of negligible concentration.

Table 7
Summary of pretreatment and challenge corrosion rates for CS and 5Cr steel specimens pretreated in TCI + DDS. In each experiment, three specimens of each metallurgy were used for weight loss analysis to measure corrosion rates. Corrosion rates are presented in the following format: average corrosion rate (maximum corrosion rate, minimum corrosion rate).

Metallurgy	Pretreatment Corrosion Rate (mm/y)	Challenge Corrosion Rate (mm/y)	Bare Steel TAN 3.5 Corrosion Rate (mm/y)
CS	0.6 (0.7, 0.5)	8.6 (8.8, 8.4)	7.8 (8.1, 7.6)
5Cr	0.9 (1.0, 0.8)	0.4 (0.3, 0.5)	1.8 (2.0, 1.6)

lications, the corrosion by crude oil fractions with both NAP and sulfur compounds lead to the formation of an oxygen-containing layer underneath the sulfide layer. It can be explained by the following process. First, sulfur compounds corrode the steel and iron sulfide layer is formed according to Eq. (2). NAP diffuses through the iron sulfide layer and corrodes the steel, leading to the formation of oil-soluble iron naphthenate (Eq. (1)). The iron naphthenate has to desorb from the steel surface and diffuse through the iron sulfide layer in order to reach the bulk solution. Given the twice size of the corresponding NAP, iron naphthenate is expected to diffuse much more slowly than the NAP and resides on the steel surface for a longer time. Thus, the iron naphthenate decomposes underneath the iron sulfide layer following Eqs. (4) & (5) and the magnetite is formed. Concurrently, the corrosion by sulfur compounds in crude oil fractions still proceeds underneath the iron sulfide layer following Eqs. 2 & 3. Therefore, the inner layer containing both magnetite and iron sulfide is formed. It seems that the composition of the inner layer relates to the content of NAP and sulfur compounds in the crude oil fraction. After the corrosion by Fraction 1 (a high-TAN/low-sulfur crude oil fraction), magnetite is the dominant component in the inner layer while the corrosion by Fractions 2 and 3 with considerable content of sulfur compounds results in inner layers of mixed magnetite and iron sulfide.

Note that the protectiveness of the oxygen-containing layer varied among different crude oil fractions. For instance, the oxygen-containing layer formed on CS specimens in Fraction 2 was much more protective than that formed in Fractions 1 and 3. The oxygen-containing layer with magnetite acted as a diffusion barrier and deterred the corrosion, but corrosion may still take place. Molecules of NAP and/or sulfur compounds may diffuse through cracks and cavities in the inner layer and corrode the steel underneath. Iron atoms in the steel matrix may diffuse through the inner layer by solid state diffusion and react with NAP and/or sulfur compounds on the interface between the inner layer and the fluid. Detailed mechanism is still being studied in our group.

The presence of chromium enhances the scale protectiveness for crude oil fractions. In the NAP corrosion, a protective chromium oxide scale has been observed on the surface of pure chromium [39,40]. Protective chromium oxide scales are commonly formed on high-chromium alloys (chromium content higher than 9%) [41–43]. In the present study, it has been found that chromium is enriched in the oxygen-containing layer on the 5Cr steel surface and enhances the scale protectiveness significantly. In literature, it has been reported that the presence of chromium in the oxygen-containing layer deters the solid diffusion of atoms [44,45]. The bond energy of Cr—O is much higher than that of Fe-O, which may help stabilize the oxygen-containing layer and enhance its protectiveness [46]. Chromium may "catalyse" the thermal decomposition of iron naphthenates and facilitate the formation of magnetite. The mechanism is still being studied in our group.

In order to verify the proposed mechanism of magnetite formation, indigenous NAP in real crude oil fractions is extracted to corrode specimens and magnetite is also found. The kinetics of NAP corrosion and corrosion by sulfur compounds for different

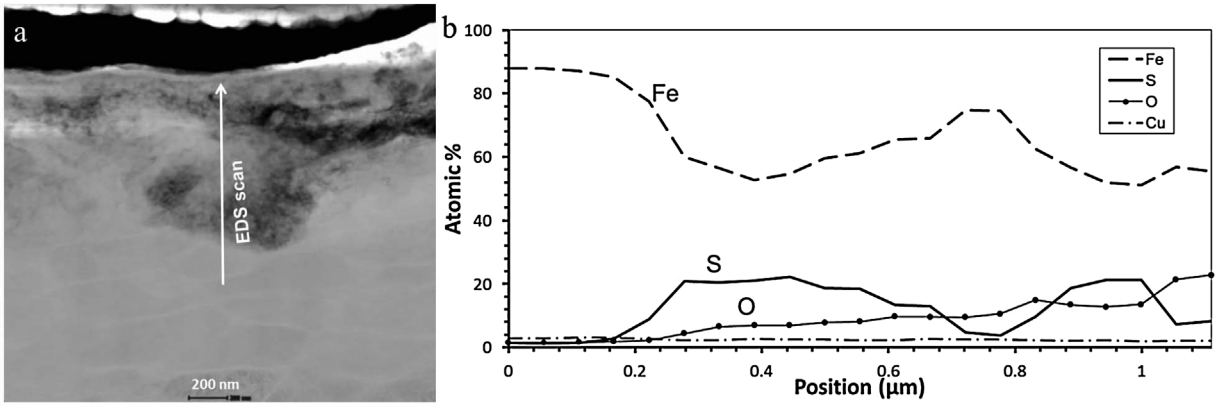

Fig. 16. Energy Dispersive Spectroscopy (EDS) scanning analysis of the inner scale formed on CS specimen pretreated in Fraction 3 (Transmission Electron Microscopy (TEM) image presented in Fig. 14). (a) Enlarged image of the inner layer; (b) Results of EDS analysis containing all detected elements. All other elements are of negligible concentration.

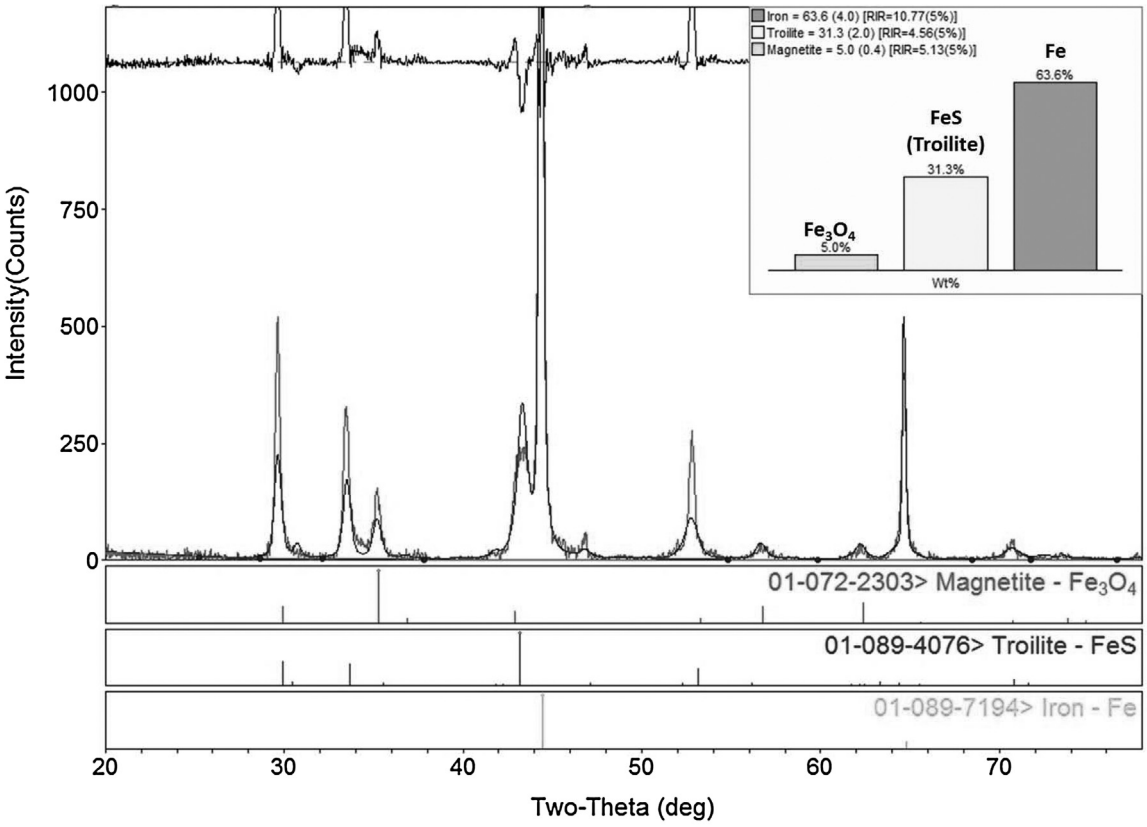

Fig. 17. Bulk X-ray Diffraction analysis of CS specimen pretreated in Fraction 3.

metallurgies are also being studied. These results in our on-going research will be published in separated publications.

5. Conclusions

In our prior publications, the protective magnetite layer adjacent to the steel surface was formed in the corrosion by a pure carboxylic acid (model NAP). In the current study, it is the first time to report the formation of magnetite in the corrosion by real crude oil fractions with complex components under refinery conditions. It is further postulated that the formation of magnetite relates to the presence of indigenous NAP in crude oil fractions, consistent with the findings relating to the corrosion by model NAP. Iron naphthenates (the product of NAP corrosion) may decompose at high temperatures and form magnetite.

However, the scale structure formed in the real crude oil fractions with NAP and sulfur compounds is different from that found in model NAP reported in our prior publications. A layer composed of magnetite only was formed in model NAP while in current research, the inner oxygen-containing layer(s) contained both iron sulfide and magnetite and the outer layer was composed of iron sulfide only. It was postulated that the outer layer of iron sulfide formed first, and decomposition of iron naphthenates and corrosion by sulfur compounds proceeded concurrently underneath it. Thus, the inner layer containing both magnetite and iron sulfide was formed. It was also found that the composition of the inner layer related to the content of NAP and sulfur compounds in crude oil fractions.

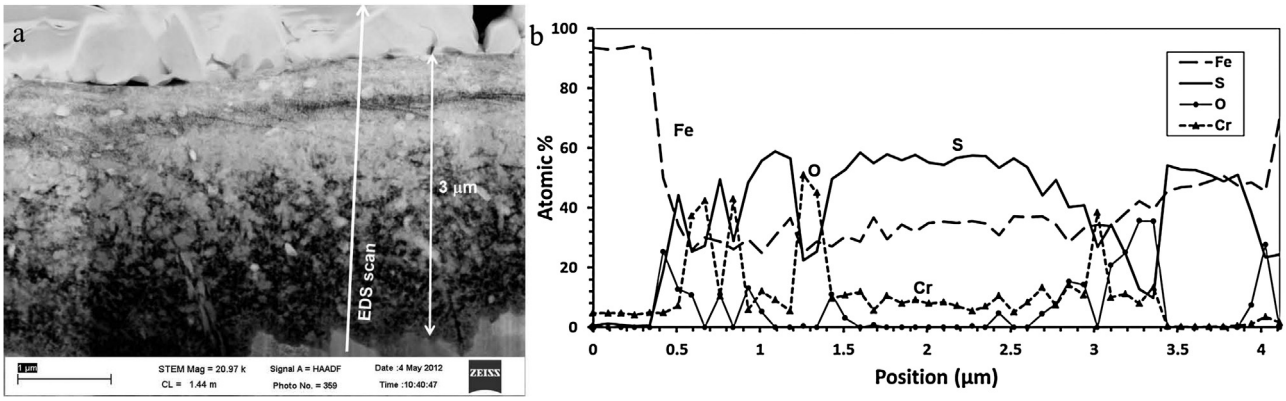

Fig. 18. Transmission Electron Microscopy (TEM)/Energy Dispersive Spectroscopy (EDS) analysis of cross-section 5Cr specimen pretreated in TCI + DDS. (a) TEM image of scale with the EDS scanning line from the bottom to the top; (b) Results of EDS analysis containing all detected elements. All other elements are of negligible concentration.

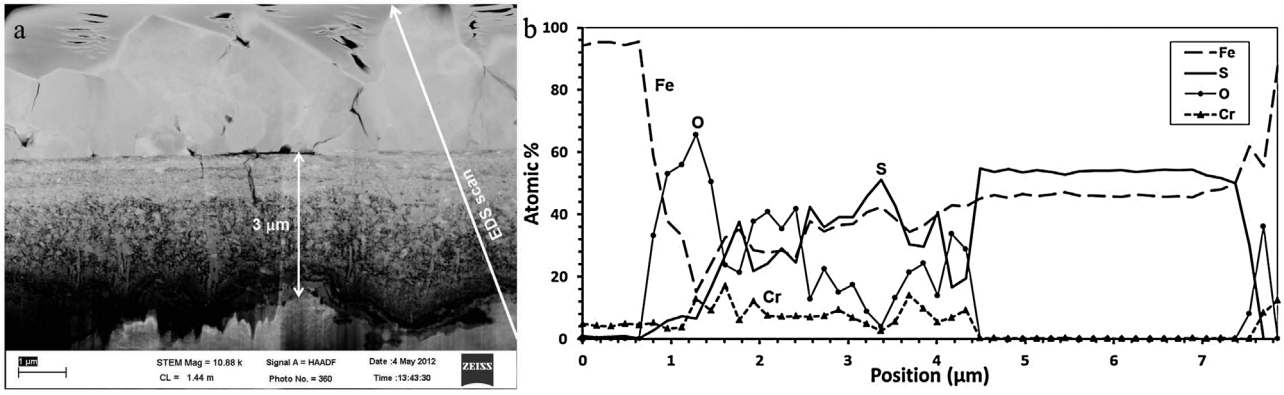

Fig. 19. Transmission Electron Microscopy (TEM)/Energy Dispersive Spectroscopy (EDS) analysis of cross-section 5Cr specimen pretreated in TCI + DDS and challenged with the corrosive TAN 3.5 solution. (a) TEM image of scale with the EDS scanning line from the bottom to the top; (b) Results of EDS analysis containing all detected elements. All other elements are of negligible concentration.

Low content of chromium in 5Cr steel significantly increased the protectiveness of the oxygen-containing layer. Probably it was due to the higher bond energy of Cr—O comparing with that of Fe—O. Chromium may "catalyse" the thermal decomposition of iron naphthenates. On-going research is investigating the effect of chromium on enhancing the protectiveness of the oxygen-containing layer.

Acknowledgements

This work was supported by Naphthenic Acid Corrosion Project in the Institute for Corrosion and Multiphase Technology, Ohio University

Authors would like to thank Dr. Yi-Yun Li from The Ohio State University for her help with TEM analysis.

References

[1] R.A. Cataldi, A.E. Hansberger, Estimating the corrosivity of crude oils, Petroleum Refiner 32 (1953) 146–150.
[2] W.A. Derungs, Naphthenic acid corrosion—an old enemy of the petroleum industry, Corrosion 12 (1956) 617–622.
[3] E. Slavcheva, B. Shone, A. Turnbull, Review of naphthenic acid corrosion in oil refining, Br. Corros. J. 34 (1999) 125–131.
[4] H.D. Dettman, N. Li, J. Luo, Refinery Corrosion, Organic Acid Structure, and Athabasca Bitumen, NACE, Houston, TX, USA, 2009 (Corrosion/2009, Paper No. 9336).
[5] A.E. Turnbull, E. Slavcheva, B. Shone, Factors controlling naphthenic acid corrosion, Corrosion 54 (1998) 922–930.
[6] R.L. Piehl, Naphthenic acid corrosion in crude distillation units, Mater. Perform. 44 (1988) 37–43.
[7] R.D. Kane, M.S. Cayard, A Comprehensive Study on Naphthenic Acid Corrosion, NACE, Houston, TX, USA, 2002 (Corrosion/2002, Paper No. 02555).
[8] O. Yepez, Influence of different sulfur compounds on corrosion due to naphthenic acid, Fuel 84 (2005) 97–104.
[9] D.R. Qu, Y.G. Zheng, H.M. Jing, X. Jiang, W. Ke, Erosion-corrosion of Q235 and 5Cr1/2Mo steels in oil with naphthenic acid and/or sulfur compound at high temperature, Mater. Corros. 56 (2005) 533–541.
[10] P. Jin, F. Farelas, W. Robbins, G. Bota, S. Nesic, Generation of H2S by crude fractions at high temperature Abstracts Of Papers Of The American Chemical Society, Vol. 248, Amer Chemical Soc, Washington, DC, 2014, pp. 544–545 (2014 Aug 10).
[11] D.R. Qu, Y.G. Zheng, H.M. Jing, Z.M. Yao, W. Ke, High temperature naphthenic acid corrosion and sulphidic corrosion of Q235 and 5Cr1/2Mo steels in synthetic refining media, Corros. Sci. 48 (2006) 1960–1985.
[12] B.S. Huang, W.F. Yin, D.H. Sang, Z.Y. Jiang, Synergy effect of naphthenic acid corrosion and sulfur corrosion in crude oil distillation unit, Appl. Surf. Sci. 259 (2012) 664–670.
[13] V. Kanukuntla, D. Qu, S. Nesic, A. Wolf, Experimental Study of Concurrent Naphthenic Acid and Sulfidation Corrosion, NACE, Houston, TX, USA, 2009 (Corrosion/2009, Paper No. 2764).
[14] P. Jin, S. Nesic, H.A. Wolf, Analysis of corrosion scales formed on steel at high temperatures in hydrocarbons containing model naphthenic acids and sulfur compounds, Surf. Interface Anal. 47 (2015) 454–465.
[15] P. Jin, W. Robbins, G. Bota, S. Nesic, Characterization of iron oxide scale formed in naphthenic acid corrosion, in: D. Firrao, M. Zhang, Z. Peng, J.P. Escobedo-Diaz, C. Bai (Eds.), Characterization of Minerals, Metals, and Materials 2016, Wiley, Tennessee, 2016, pp. 115–125.
[16] P. Jin, Mechanism of Corrosion by Naphthenic Acids and Organosulfur Compounds at High Temperatures, Ohio University, 2013 (Ph.D. Dissertation).
[17] H.A. Wolf, F. Cao, S.C. Blum, A.M. Schilowitz, S. Ling, J.E. McLAUGHLIN, S. Nesic, P. Jin, B. Gheorghe, Method for identifying layers providing corrosion protection in crude oil fractions, U.S. Patent 9140640, (2015).
[18] P. Jin, W. Robbins, G. Bota, S. Nesic, Characterization of magnetite scale formed in naphthenic acid corrosion, JOM. doi: 10.1007/s11837-016-2164-y10.1007/s11837-016-2164-y.
[19] P. Jin, W. Robbins, G. Bota, Mechanism of magnetite formation in high temperature corrosion by model naphthenic acids, Corros. Sci. 111 (2016) 822–834.

[20] P. Jin, G. Bota, W. Robbins, S. Nesic, Analysis of oxide scales formed in the naphthenic acid corrosion of carbon steel, Energy Fuels 30 (2016) 6853–6862.
[21] M. Renz, Ketonization of carboxylic acids by decarboxylation: mechanism and scope, Eur. J. Org. Chem. 2005 (2005) 979–988.
[22] L.J. Goossen, P. Mamone, C. Oppel, Catalytic decarboxylative cross-ketonisation of aryl-and alkylcarboxylic acids using magnetite nanoparticles, Adv. Synth. Catal. 353 (2011) 57–63.
[23] G. Kataby, M. Cojocaru, R. Prozorov, A. Gedanken, Coating carboxylic acids on amorphous iron nanoparticles, Langmuir 15 (1999) 1703–1708.
[24] C.J. Chen, H.Y. Lai, C.C. Lin, J.S. Wang, R.K. Chiang, Preparation of monodisperse iron oxide nanoparticles via the synthesis and decomposition of iron fatty acid complexes, Nanoscale Res. Lett. 4 (2009) 1343–1350.
[25] N.R. Jana, Y. Chen, X. Peng, Size-and shape-controlled magnetic (Cr, Mn Fe, Co, Ni) oxide nanocrystals via a simple and general approach, Chem. Mater. 16 (2004) 3931–3935.
[26] K.S. Salih, P. Mamone, G. Dörr, T.O. Bauer, A. Brodyanski, C. Wagner, M. Kopnarski, R.N. Klupp Taylor, S. Demeshko, F. Meyer, V. Schünemann, Facile synthesis of monodisperse maghemite and ferrite nanocrystals from metal powder and octanoic acid, Chem. Mater. 25 (2013) 1430–1435.
[27] C.J. Chen, R.K. Chiang, H.Y. Lai, C.R. Lin, Characterization of monodisperse wüstite nanoparticles following partial oxidation, J. Phys. Chem. C 114 (2010) 4258–4263.
[28] F.X. Redl, C.T. Black, G.C. Papaefthymiou, R.L. Sandstrom, M. Yin, H. Zeng, C.B. Murray, S.P. O'Brien, Magnetic, electronic, and structural characterization of nonstoichiometric iron oxides at the nanoscale, JACS 126 (2004) 14583–14599.
[29] J. Fukushima, K. Kodaira, T. Matsushita, Preparation and formation process of various iron oxide films by thermal decomposition of iron naphthenate, J. Ceram. Soc. Jpn. 84 (1976) 529–533.
[30] Y. Konishi, T. Kawamura, S. Asai, Preparation and characterization of fine magnetite particles from iron (III) carboxylate dissolved in organic solvent, Ind. Eng. Chem. Res. 32 (1993) 2888–2891.
[31] W. Wu, Z. Wu, T. Yu, C. Jiang, W.S. Kim, Recent progress on magnetic iron oxide nanoparticles: synthesis, surface functional strategies and biomedical applications, Sci. Tech. Adv. Mater. 16 (2015) 1–43.
[32] S. Stolen, R. Gloeckner, F. Gronvold, Nearly stoichiometric Iron monoxide formed as a metastable intermediate in a two-stage disproportionation of quenched wüstite. thermodynamic and kinetic aspects, Thermochim. Acta 256 (1995) 91–106.
[33] K. Qian, W.K. Robbins, C.A. Hughey, H.J. Cooper, R.P. Rodgers, A.G. Marshall, Resolution and identification of elemental compositions for more than 3000 crude acids in heavy petroleum by negative-ion microelectrospray high-field Fourier transform ion cyclotron resonance mass spectrometry, Energy Fuels 15 (2001) 1505–1511.
[34] C.S. Hsu, G.J. Dechert, W.K. Robbins, E.K. Fukuda, Naphthenic acids in crude oils characterized by mass spectrometry, Energy Fuels 14 (2000) 217–223.
[35] D.L. Mitchell, J.G. Speight, The solubility of asphaltenes in hydrocarbon solvents, Fuel 52 (1973) 149–152.
[36] P. Ajmera, W. Robbins, S. Richter, S. Nesic, The Role of Asphaltenes in Inhibiting Corrosion and Altering the Wettability of the Steel Surface, NACE, Houston, TX, USA, 2010 (Corrosion/2010, Paper No. 10329).
[37] M. El Kamel, A. Galtayries, P. Vermaut, B. Albinet, G. Foulonneau, X. Roumeau, B. Roncin, P. Marcus, Sulfidation kinetics of industrial steels in a refinery crude oil at 300C: reactivity at the nanometer scale, Surf. Interface Anal. 42 (2010) 605–609.
[38] N.R. Smart, A.P. Rance, A.M. Pritchard, Laboratory Investigation of Naphthenic Acid Corrosion Under Flowing Conditions, NACE, Houston, TX, 2002 (Corrosion/2002, Paper No. 02484).
[39] B.N. Patrick, R. Chakravarti, T.M. Devine, An acoustic microbalance study of high-temperature naphthenic acid corrosion of common iron-alloying elements, Corrosion 71 (2015) 1135–1146.
[40] B.N. Patrick, R. Chakravarti, T.M. Devine, Dynamic measurements of corrosion rates at high temperatures in high electrical resistivity media, Corros. Sci. 94 (2015) 99–103.
[41] L. Latu-Romain, Y. Madi, S. Mathieu, F. Robaut, J.-P. Petit, Y. Wouters, Advanced STEM/EDX investigation on an oxide scale thermally grown on a high-chromium iron–nickel alloy under very low oxygen partial pressure, Corros. Sci. 101 (2015) 193–200.
[42] T. Gheno, M.Z. Azar, A.H. Heuer, B. Gleeson, Reaction morphologies developed by nickel aluminides in type II hot corrosion conditions: the effect of chromium, Corros. Sci. 101 (2015) 32–46.
[43] C. Ostwald, H.J. Grabke, Initial oxidation and chromium diffusion I. Effects of surface working on 9–20% Cr steels, Corros. Sci. 46 (2004) 1113–1127.
[44] E. Schuster, K.H. Neeb, W. Ahlfänger, R. Henkelmann, R.T. Järnström, Analyses of primary side oxide layers on steam generator tubes from PWRs and radiochemical issues on the contamination of primary circuits, J. Nucl. Mater. 152 (1988) 1–8.
[45] G.C. Wood, Some observations on the break-through of protective oxide films on iron-chromium alloys, Corros. Sci. 25 (1965) 255–268.
[46] N.K. Das, T. Shoji, Y. Takeda, A fundamental study of Fe–Cr binary alloy–oxide film interfaces at 288 °C by computational chemistry calculations, Corros. Sci. 52 (2010) 2349–2352.